Mechanism of the increase in bulk modulus of perovskite $ScRh_3B_x$ by vacancies

Ryoji Sahara,* Toetsu Shishido, and Akiko Nomura
Institute for Materials Research, Tohoku University, Aoba-ku, Sendai 980-8577, Japan

Kunio Kudou
Faculty of Engineering, Kanagawa University, 3-27-1 Rokkakubashi, Kanagawa-ku, Yokohama 221-8686, Japan

Shigeru Okada
Faculty of Engineering, Kokushikan University, 4-28-1 Setagaya-ku, Tokyo 154-8515, Japan

Vijay Kumar
Research Institute for Computational Sciences (RICS), National Institute of Advanced Industrial Science and Technology (AIST), AIST Tsukuba Central 2, Umezono 1-1-1, Tsukuba 305-8568, Japan;
Institute for Materials Research, Tohoku University, Aoba-ku, Sendai 980-8577, Japan;
and Dr. Vijay Kumar Foundation, 45 Bazaar Street, K. K. Nagar (West), Chennai 600 078, India

Kazuo Nakajima and Yoshiyuki Kawazoe
Institute for Materials Research, Tohoku University, Aoba-ku, Sendai 980-8577, Japan
(Received 19 October 2005; revised manuscript received 17 January 2006; published 1 May 2006)

First-principles calculations have been performed on perovskite-type $ScRh_3B_x$ in order to understand the variation in the structural properties and bulk modulus as a function of the boron concentration. We use the projected augmented wave method with a supercell to treat different configurations of vacancies and boron atoms. The generalized gradient approximation is used for the exchange-correlation functional. The calculated lattice constants are found to be in excellent agreement with the experimental results. Maximum bulk modulus is realized surprisingly at $x=0.5$, contrary to the expectation that vacancies reduce the number of chemical bonds and hence the strength of the compounds. This is explained by examining the changes in the atomic and electronic structures upon B doping. We find that the doping enhances the cohesive energy monotonically due to the strong covalent bonding between B $2p$ and Rh $4d$ states. However, at $x=0.5$ a configuration is achieved in which each boron is surrounded by vacancies at the cube centers, and vice versa. This reduces strain in the structure and the Rh-B bonds are short, leading to a maximum in the bulk modulus. The density of states at the Fermi energy is also minimum for $x=0.5$ which adds further stability to the structure.

DOI: 10.1103/PhysRevB.73.184102 PACS number(s): 62.20.−x, 61.72.Ji

I. INTRODUCTION

An understanding of the mechanical behavior of materials is important for their applications. *Ab initio* calculations provide a microscopic framework to study the cohesion and deformation behavior of mixed systems such as oxides, borides, carbides, and nitrides. These are technologically very important due to their high stability and hardness, which make them useful for high-temperature environments, cutting tools, and hard coating applications. The nonmetal atom in these materials often has substoichiometric composition due to the existence of vacancies. This can have a significant effect on the material properties and therefore controlling the vacancy concentration in these systems is an important task. In this context perovskite-type oxides have been the subject of great attention because of their interesting properties, including superconductivity,[1] insulator-metal transition, ionic conduction characteristics,[2] and dielectric as well as ferroelectric properties.[3,4] On the other hand, only a few studies have been done on nonoxide perovskite-type compounds such as the ternary rare-earth (R) rhodium borides RRh_3B and carbides RRh_3C.[5–7] It is of interest to systematically investigate the mechanical properties of R borides RRh_3B, because boron makes many technologically important compounds with mechanical hardness. In the perovskite-type structure with space group $Pm3m$, R is at the eight corners of a cube and Rh at the six face centers, while boron, carbon, and/or vacancy occupy the center of the cube as is shown in Fig. 1 in the case of $ScRh_3B$. Changing the boron concentration by substitutional doping of carbon or

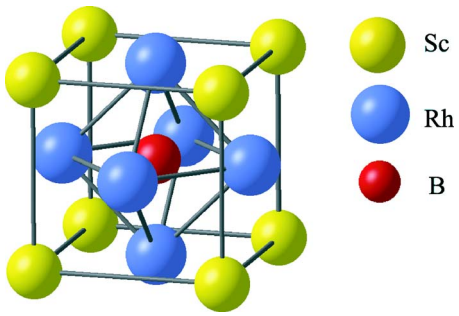

FIG. 1. (Color online) The perovskite cubic unit cell of $ScRh_3B_x$. Sc atoms are at the corners while Rh occupies face centers. B and vacancy occupy the center of the cube.

vacancy, it could be possible to change the properties of these compounds.

Shishido *et al.*[8–12] have studied experimentally the dependency of lattice parameters and hardness of *R* rhodium borides and carbides by changing the *R* atoms as well as boron stoichiometry. They obtained a decrease in the lattice parameter and an increase in the microhardness with decreasing atomic size of the *R* element. Here we consider the case of $ScRh_3B_x$ which forms a continuous solid solution in the range of $0 \leqslant x \leqslant 1$ with cubic structure (space group $Pm3m$) and exhibits a very intriguing relationship between boron concentration x and hardness in that the local maximum in microhardness is realized at around $x=0.25$. To analyze these behaviors and understand their origin from the electronic structure, we present here results of first-principles calculations for different compositions of B and vacancies.

There have been a few other studies on these systems. Among these recently Schaak *et al.*[13] have explored the formation of intermetallic boride and carbide perovskites AXM_3 (A=Mg, Ca, Sc, Y, Lu, Zr, or Nb; M=Ni, Ru, Rh, Pd, or Pt; and X=B or C) and identified the stability range by varying the compositions of B and C. For A=Sc and M=Rh, they confirmed the formation of the stoichiometric compound. Also there have been some efforts to understand hardness of materials from *ab initio* calculations. In general hardness is known to be a material parameter that indicates resistance to elastic or plastic deformation. Besides *ab initio* calculations, semiempirical studies have also been performed to describe the origin of hardness at the atomic scale as well as to develop empirical correlations that could be very helpful from the point of view of applications. However, there is no unique way[14,15] to have a quantitative description. Cohen[14] proposed a simple relationship between bulk modulus and nearest-neighbor distance for tetrahedrally bonded semiconductors such as C, Si, and Ge as well as III-V and II-VI compounds in which covalent bonding plays a dominant role. According to this relation the bulk modulus increases with decreasing nearest-neighbor interatomic distance. On the other hand ionicity tends to decrease the bulk modulus as this removes charge from the bonds and localizes it around the ions. Teter[16] has shown an empirical relationship between bulk modulus, shear modulus, and Vickers hardness using a set of different materials. It was suggested that high shear modulus is a better criterion for hardness compared to bulk modulus. Jhi *et al.*[16,17] have studied an electronic mechanism of hardness enhancement in transition metal carbonitrides such as TiC_xN_{1-x} using an *ab initio* pseudopotential approach. They showed that the highest hardness of TiC_xN_{1-x} is realized when valence electron concentration is about 8.4 electrons per cell. It originates from the complete filling of the shear-resistive $pd\sigma$ bonding states at this electron concentration. They also analyzed the effects of vacancies on the mechanical properties of the transition metal carbides and nitrides[18] and showed that the vacancy produces entirely different effects on the mechanical strength of groups IVb nitrides and Vb carbides. Here it is worth noting that although the elastic properties are regarded as a measure of hardness of materials, it is not always positively correlated with the experimentally measured Vickers hardness.

The electronic structure of some borides including YRh_3B which is of the same type as those under consideration in this study has been studied by Ravindran *et al.*[19] using tight-binding linear muffin-tin orbital method. YRh_3B is isoelectronic to $ScRh_3B$ and the Fermi level was found to lie in a region of high density of states. This was used to explain the occurrence of superconductivity in this compound. They also reported the existence of covalent bonding between Rh and B in these compounds. Oku *et al.*[20] studied $ScRh_3$ and $ScRh_3B$ stoichiometric compounds using ultrasoft pseudopotentials and a plane wave basis set and compared their results with x-ray photoelectron spectroscopy spectra and Knight shift measurements. However, they did not study the mechanical properties of these compounds. Recently Music *et al.*[21] have studied 20 stoichiometric RM_3B perovskite borides with $M=4d$ metals and R=Sc or Y, using ultrasoft pseudopotentials and a plane wave basis set. They studied the bonding character as well as the bulk and shear moduli of these compounds. The latter were found to peak at M=Rh for R=Y, and for R=Sc the highest value of bulk modulus of 216 GPa was obtained for M=Ru and an only slightly smaller value of 210 GPa for M=Rh.

In an earlier study Sahara *et al.*[22] performed *ab initio* calculations on perovskite-type RRh_3B and RRh_3C (R=Sc, Y, or La) to obtain their equilibrium lattice constants and elastic properties such as the elastic constants, bulk moduli, shear moduli, and Young's moduli. The calculated lattice constants were in excellent agreement (within 1%) with experimental results. The bulk modulus in these compounds increases with a decrease in the lattice parameter, and following Cohen's proposal,[14] a new relationship between the bulk modulus and the nearest-neighbor distance was also proposed for these systems. However, these theoretical studies are limited to stoichiometric compounds. In the present study, we consider a series of *R* rhodium borides $ScRh_3B_x$ with varying x and study their elastic properties from total energy calculations in order to understand the effects of vacancies on the mechanical strength of these compounds.

In Sec. II we discuss our calculation procedure while the results are given in Sec. III. A summary of our results is given in Sec. IV.

II. METHOD OF CALCULATION

We use the projected augmented wave method[23,24] with the Vienna *ab initio* simulation program (VASP).[25–27] Minimization of the free energy over the degrees of freedom of the electron density and atomic positions is performed using the conjugate gradient iterative minimization technique.[28] The exchange-correlation energy has been calculated within the generalized gradient approximation (GGA).[29] The atomic positions and structural parameters are fully optimized using the conjugate gradient method. The cutoff energy for the plane wave expansion is taken to be 318.59 eV, which is large enough to obtain good convergence. A higher cutoff value of 414.167 eV for $x=0.5$ and 1.0 led to negligible changes in the lattice parameters and about 0.5% change in the bulk modulus. For Brillouin zone integrations, we use $4\times4\times4$ **k** points, which is also large enough to obtain good convergence. Tests were made by using $8\times8\times8$ **k** points and this again led to negligible changes in the lattice param-

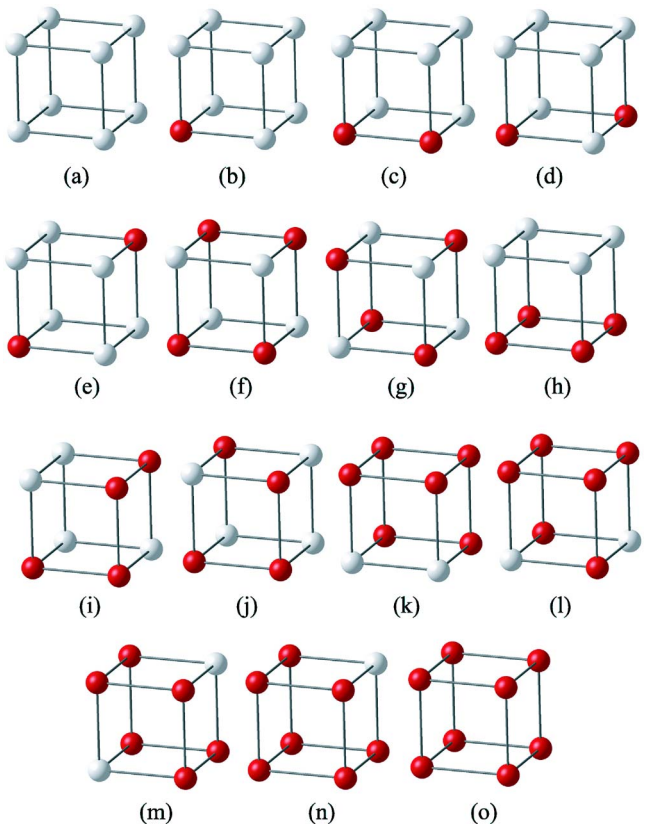

FIG. 2. (Color online) Different configurations of boron and vacancies in a $2\times2\times2$ supercell of $ScRh_3B_x$ for x=(a) 0, (b) 0.125, (c)–(e) 0.25, (f)–(j) 0.5, (k)–(m) 0.75, (n) 0.875, and (o) 1 used in the present calculations. Only the sublattice sites that nonmetal atoms and vacancies occupy and which correspond to the body-center sites of the cubic perovskite cells, are shown. Dark (red) and white balls correspond to B and vacancy, respectively.

eter as well as small changes in the bulk modulus for $x=0.5$ and 1. Therefore, all other calculations have been done using $4\times4\times4$ **k** points. Further, we studied the effects of taking into account spin polarization but the change in energy as well as the magnetic moments were found to be negligible. A similar conclusion has also been reached by Music *et al.*[21] Therefore all other calculations have been done without considering spin polarization.

In order to describe substoichiometric concentrations, we use a $2\times2\times2$ supercell of the perovskite structure. Recall that compounds with vacancies have been experimentally found to exist in perovskite-type structures with space group $Pm3m$ in the whole range of boron concentration of $0\leqslant x\leqslant1$. Different possible distributions of vacancies for a given concentration of B are considered within the supercell to determine energetically the most favorable distribution. Figure 2 shows these configurations for $ScRh_3B_x$. Here only sublattice sites of the nonmetal atoms B and vacancies, which correspond to the body-center sites of the cubic perovskite cell, are shown. Starting from the two limiting cases of x=0 and 1 [Figs. 2(a) and 2(o), respectively] we have considered cases with x=0.125 (b), 0.25 (c)–(e), 0.50 (f)–(j), 0.75 (k)–(m), and 0.875 (n).

The bulk modulus B defined as

$$B=-\frac{Vdp}{dV}=\frac{V\,d^2E_{tot}(V)}{dV^2}, \tag{1}$$

where V is the volume of the cell, and p, the pressure, is calculated from the Murnaghan equation of state[30]

$$E_{tot}(V)=\frac{B_0V}{B_0'(B_0'-1)}\left[B_0'\left(1-\frac{V_0}{V}\right)+\left(\frac{V_0}{V}\right)^{B_0'}-1\right]+E_{tot}(V_0). \tag{2}$$

Here $E_{tot}(V)$ is the total energy of the system at volume V, and B_0 and B_0' are the bulk modulus and its pressure derivative at the equilibrium volume V_0, respectively. In the present study, $E_{tot}(V)$ is calculated for cubic perovskite cells at 13 different volumes and the values are fitted with Eq. (2). In a few cases we also obtained the bulk modulus by fitting the energy vs volume curve to a third-degree polynomial as done by Music *et al.*[21] This leads to a slightly higher value of the bulk modulus as compared to the value obtained from Eq. (1). Furthermore, we perform two types of calculations using cubic structure as initial condition: (1) by keeping the cubic structure because the experimental results show that these compounds keep the cubic structure for all boron concentrations, and (2) by optimizing structure allowing changes in the lattice parameters to check the stability of the cubic cell, especially for the low-symmetric case.

III. RESULTS AND DISCUSSION

Table I shows the initial and optimized structural parameters obtained from the two methods of optimizations. It is noted that for the cases of x=0 (a), 0.125 (b), 0.875 (n), 1 (o), and the lowest-energy distributions for B substoichiometries with x=0.25, 0.5, and 0.75, the structure remains cubic. In these cases, the B atoms are the farthest from each other except for the case of x=0.75 and are symmetrically distributed. For x=0.75, the energy difference between configurations (l) and (m) in Fig. 2 is quite small. The changes in the lattice parameters obtained from the optimization of the stresses and from the Murnaghan equation of state assuming cubic structure in all cases, are small. This also reflects good accuracy of the calculations. For the higher-energy configurations, there are noncubic distortions in the optimized structures, but generally these are also small, the maximum value being 5%. This is caused by the presence of B atoms at the nearest sites that leads to an increase in the corresponding lattice parameters. In a real system the B atom and vacancy distribution may not be perfectly ordered. A random distribution would lead to a cubic structure on an average as observed. We have therefore calculated the mean cubic lattice parameter in the cases of noncubic distortions and these again agree very closely with the values obtained from the Murnaghan equation of state assuming a cubic structure. The bulk modulus is found to have the highest value for the lowest-energy isomer in general for each substoichiometric boron concentration.

As experimental results show a cubic structure over the whole composition of B, we have shown in Fig. 3 the relationship between the calculated equilibrium lattice constant

TABLE I. Initial and optimized structural parameters in angstroms, and the bulk modulus. Indexing of the configuration is defined in Fig. 2. For the final structure, results are given for the two methods used for the optimization of the unit cell, one in which all the lattice parameters are optimized and the other in which the cubic structure is kept for all concentrations. Bulk modulus is given for the cubic structure.

	Initial structural parameter	Final structural parameter					
		Optimized cell parameter					
x	Cubic structure a axis	a axis	b axis	c axis	Mean lattice parameter	Cubic structure a axis	Bulk modulus (GPa)
0.000 (a)	7.850	7.849	7.849	7.849	7.849	7.856	190
0.125 (b)	7.900	7.895	7.895	7.895	7.895	7.900	192
0.250 (c)	7.950	8.093	7.875	7.875	7.947	7.954	191
0.250 (d)	7.950	7.964	7.964	7.890	7.939	7.943	194
0.250 (e)	7.950	7.936	7.936	7.936	7.936	7.940	195
0.500 (f)	8.050	8.206	7.947	7.947	8.032	8.043	194
0.500 (g)	8.050	8.023	8.023	8.023	8.023	8.028	198
0.500 (h)	8.050	8.190	8.190	7.779	8.051	8.063	190
0.500 (i)	8.050	8.043	8.043	8.059	8.048	8.052	192
0.500 (j)	8.050	8.107	7.903	8.107	8.038	8.044	194
0.750 (k)	8.150	8.206	8.121	8.121	8.149	8.157	193
0.750 (l)	8.150	8.138	8.138	8.150	8.142	8.149	195
0.750 (m)	8.150	8.144	8.144	8.144	8.144	8.148	194
0.875 (n)	8.200	8.195	8.195	8.195	8.195	8.201	196
1.000 (o)	8.250	8.244	8.244	8.244	8.244	8.250	197

for cubic structures and boron concentration x. It shows that the lattice constant increases monotonically as x increases and that the calculated values are in excellent agreement (within 1%) with the experimental results. There is a slight overestimation of the lattice constant for the whole concentration range which is often a feature of the GGA. In the case of $x=1$, our value of the lattice constant (4.125 Å) is in excellent agreement with the other theoretical value (4.132 Å) obtained by Music *et al.*[21]

The calculated equilibrium volume of $ScRh_3B_x$ nearly obeys the Vegard law $V_{eq}(x)=xV_{eq}^{ScRh_3B}+(1-x)V_{eq}^{ScRh_3}$. The cohesive energy for different x and for different distributions of B atoms and vacancies is shown in Fig. 4. We have given the values obtained by assuming cubic unit cells as well as for the optimized cells. The difference in the two cases is small. The cohesive energy for a given concentration x differs depending on the distribution of B and vacancies. The variation is appreciable at $x=0.25$, 0.5, and 0.75. The energetically most stable configurations of B atoms and vacancies at these concentrations are shown in Figs. 2(e), 2(g), and 2(l), respectively. The energy differences between the most stable and the second most stable configurations are 1.03×10^{-1}, 1.46×10^{0}, and 1.48×10^{-1} eV per supercell at $x=0.25$, 0.5, and 0.75, respectively. The results for the lowest-energy configurations show that the cohesive energy increases almost linearly up to $x=0.5$ and the increase is quite significant. Thereafter there is a small decrease and then again a small increase. It is also noteworthy that the other configurations of B and vacancy distribution lie significantly higher in energy for $x=0.5$.

Figure 5 shows the variation of the bulk modulus with boron concentration. Again, results for all the calculated configurations are shown and these reflect the behavior found for the cohesive energy. The configuration with the highest bulk

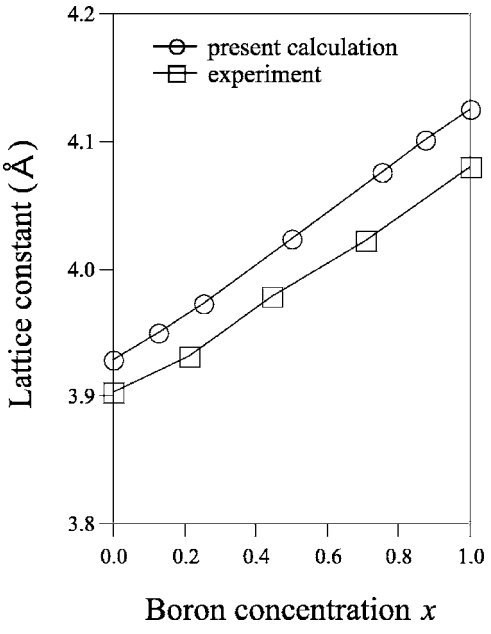

FIG. 3. Relationship between cubic lattice constant and boron concentration. Open circles correspond to the present results while open squares are the experimental data from Refs. 8 and 11.

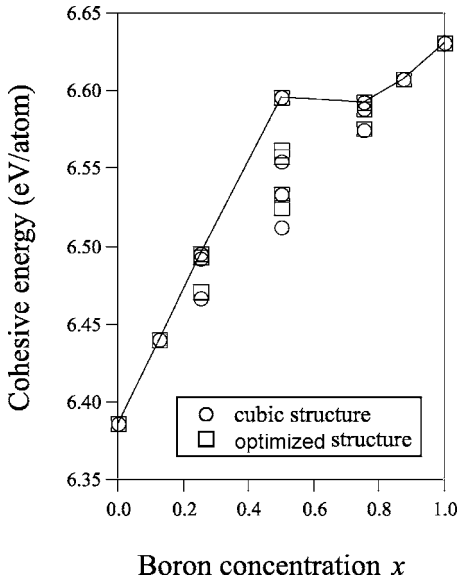

FIG. 4. Relationship between the cohesive energy per atom and boron concentration x. Values are given for both the cases (1) considering cubic unit cells and (2) where the unit cell parameters have been optimized. The optimization increases the cohesive energy slightly. The values corresponding to the highest cohesive energy configurations for a given x have been connected by a line to show the trend. Different points for a given x correspond to the different distributions of B and vacancies (see Fig. 2).

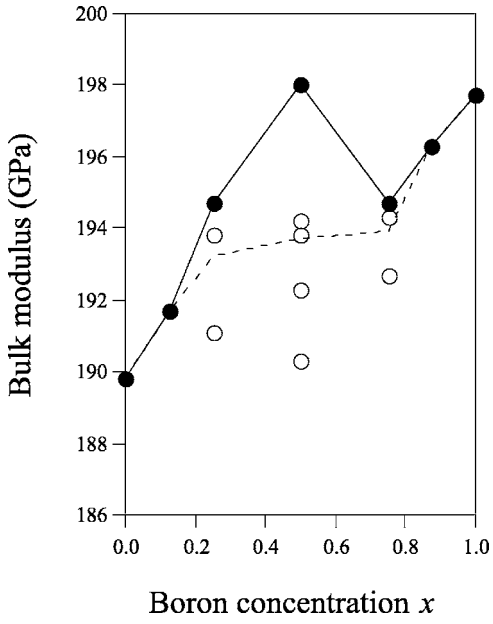

FIG. 5. Relationship between the bulk modulus and boron concentration. Open circles show the results for all the configurations calculated in the present study. Solid circles correspond to the configuration with the lowest energy for each boron concentration.

modulus also corresponds to the highest cohesive energy in Fig. 4 and hence the most stable configuration for each boron concentration in general. There is significant configuration dependence of the bulk modulus for each substoichiometric concentration x. We find that the highest bulk modulus is obtained at $x=0.5$, though the cohesive energy is the highest for $x=1$. This value is close to the results obtained for the case of $x=1$. For $x=0.5$, the highest value of bulk modulus is realized with the configuration shown in Fig. 2(g) where boron atoms occupy the body-center sites of perovskite structure in a tetrahedral arrangement such that on this sublattice each boron is surrounded by vacancies, and vice versa. For the case of $x=1$, our value of the bulk modulus, 197 GPa, is lower than the value (210 GPa) obtained by Music *et al.*[21] This difference is likely to be due to the different procedure used by them to obtain the bulk modulus. In our calculations, an increase in the number of **k** points from $8\times8\times8$ to $12\times12\times12$ changes the value of the bulk modulus to 199 GPa which reflects good convergence of our calculations. However, when we used third-order polynomial fitting of the total energy with volume as it was done by Music *et al.*, we obtained the bulk modulus for $12\times12\times12$ **k** points to be 203 GPa. This result will also depend on the number of points fitted in the curve.

As B vacancies reduce the number of chemical bonds as well as the cohesive energy, it could be expected that they reduce the strength of a material. However, if bulk modulus is taken to be a criterion for the hardness of the compounds then $ScRh_3B_x$ does not follow this simple picture. The question is then how effectively vacancies in these compounds contribute to the enhancement of the bulk modulus. To clarify the origin, we studied the variation in the electronic structure of $ScRh_3$ as well as the changes in the local atomic structure due to the doping of B. Figure 6 shows the total and the site-projected density of states (DOS) along with the angular momentum decomposition for (a) $ScRh_3$, (b) $ScRh_3B_{0.5}$, and (c) $ScRh_3B$ as examples. In the case of $ScRh_3B_{0.5}$, the results are shown for the energetically most stable configuration with the highest bulk modulus [see Fig. 2(g)].

Figure 6(a) shows the total and the partial DOS for $ScRh_3$. The main contribution to the total DOS comes from the d orbitals of Rh. The $4s$ and $4p$ orbitals of Sc have significant charge transfer to Rh as will be further clear from the discussion of the charge density distribution later. The $3d$ orbitals of Sc hybridize with those of Rh and contribute significantly to the DOS, but most of the occupied states are the Rh $4d$ states. Therefore the bonding between Sc and Rh could be said to be ionic with some covalent character. These general features of the Sc and Rh bonding also exist in other cases when B is doped, but the $3d$ contribution from Sc is slightly reduced and the $3d$ Sc peak above the Fermi energy increases slightly; thereby the ionic contribution to the bonding is slightly increased. As boron is added, a peak appears at the bottom of the band and it can be seen in the total and partial DOSs of boron in Figs. 6(b) and 6(c). This is derived from the boron $2s$ orbital and it has little hybridization with the Rh or Sc states. However, the $2p$ orbitals of boron hybridize strongly with the $4d$ orbitals of Rh and there is a strong bonding peak (at around -5 eV) near the bottom of the d band and it contributes dominantly to the bonding as some of the $4d$ states of Rh are pulled down. The antibonding hybridized states can be seen above the Fermi level and these nearly overlap with the Sc $3d$ states. These features grow and become broader with increasing boron concentration [Fig.

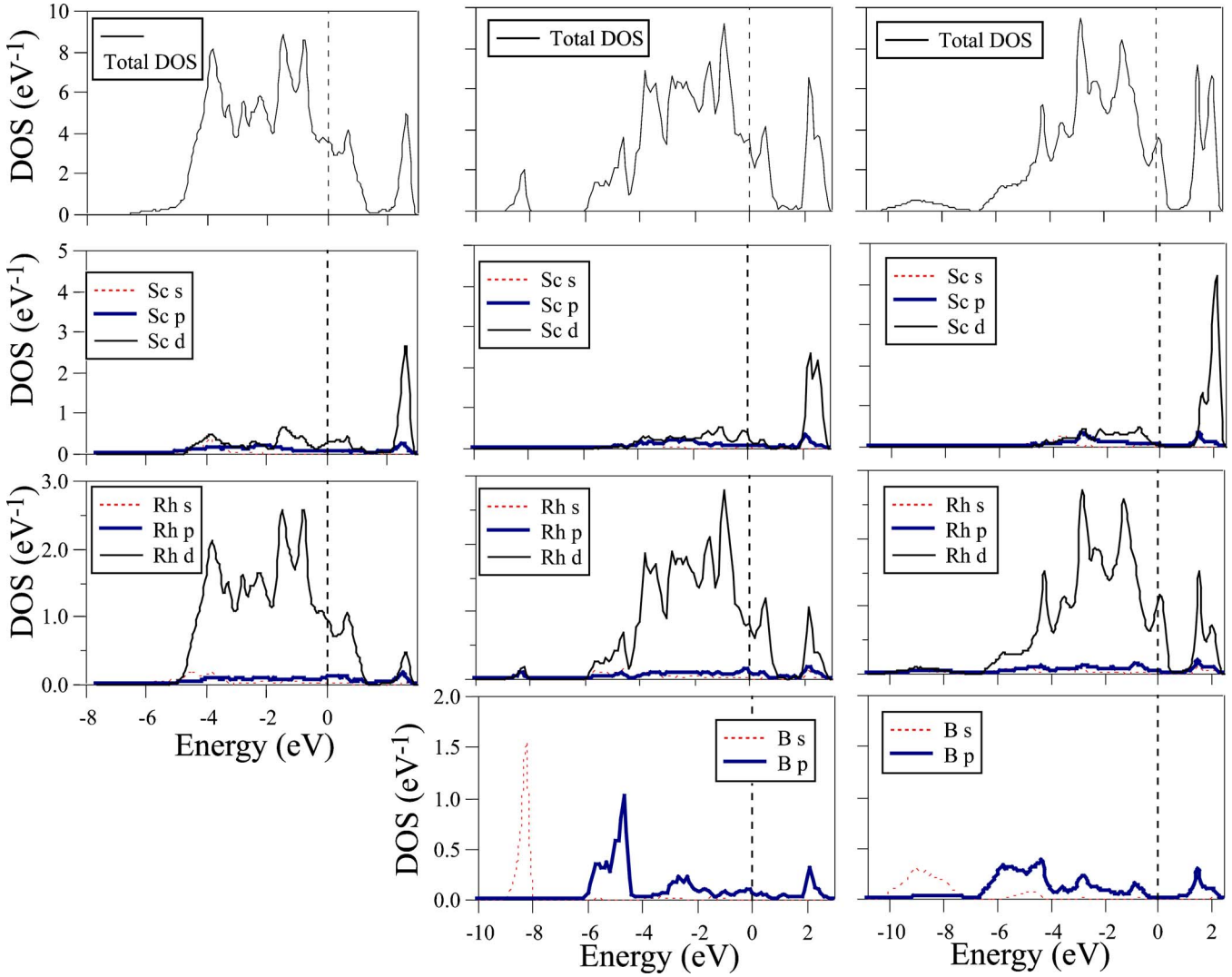

FIG. 6. (Color online) Total density of states and the site-projected partial density of states for (a) $ScRh_3$, (b) $ScRh_3B_{0.5}$ (highest cohesive energy configuration), and (c) $ScRh_3B$. Fermi energy lies at the energy zero.

6(c)] and have also been found in other distributions of boron and vacancies. Comparing the DOS in the three cases, it can be seen that the Fermi level has moved upward as if filling a rigid band by doping of electrons due to B atoms.

Interestingly the total DOS as well as the partial DOS of Rh 4*d* states at the Fermi energy decrease as x increases and these are the lowest at $x=0.5$ (Fig. 7), beyond which there is again an increase. The partial DOSs of Sc 3*d* and B 2*p* states contribute relatively little to the total DOS at the Fermi energy. The DOS provides a general feature of the bonding in these compounds, which is predominantly the strong covalent bonding between B 2*p* and Rh 4*d* orbitals. This leads to increasing cohesive energy with increasing boron concentration in general as we find except for $x=0.75$. In all cases the compounds are metallic but the DOS suggests that substitutional doping with C could make them semiconducting or semimetallic. Indeed we find that for $ScRh_3C$, the Fermi energy lies in a pseudogap.[31]

The electronic charge density in the (001) plane passing through Rh and B ions is shown in Figs. 8(a), 8(c), and 8(d) for $x=0$, 0.5, and 1, respectively and in the (011) plane in Fig. 8(b) for $x=0$. These data support the covalent bonding nature between B and Rh atoms as described above. For $ScRh_3$ [Figs. 8(a) and 8(b)] most of the charge is found around the Rh ions and little at the center of the cube [Fig. 8(a)] or around the Sc ions. Doping of boron atoms leads to covalent bonding with the neighboring Rh atoms and small changes in the charge distribution around those Rh ions that are nearest neighbors to a vacancy. Figure 8(c) shows the charge density for $ScRh_3B_{0.5}$ where only Rh and B can be seen. As the boron concentration increases to 1, the same behavior continues [Fig. 8(d)].

Further insight about the effects of doping is obtained from the relaxation of Rh ions when B is doped. From Fig. 3, we note a continuous increase in the lattice constant with B doping (see also Table II). However, because of our use of a supercell and the relaxation of ions, we can also see the displacements of different ions as x changes. It is noted that the doping of B atoms displaces the neighboring Rh ions. Comparing the case of $x=0$, there is an increase in the bulk modulus up to $x=0.5$ in the lowest-energy configurations due to the formation of strong covalent bonds between Rh and B.

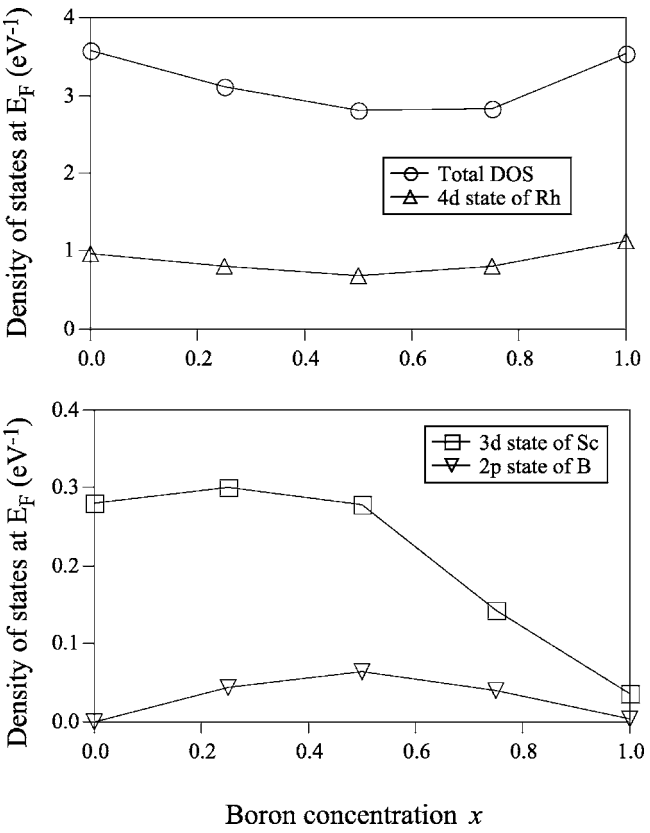

FIG. 7. The variation of the density of states at the Fermi energy as a function of x.

Up to $x=0.5$ all Sc ions are at the lattice positions but Rh ions with a B atom as nearest neighbor are displaced outward of the corresponding cubic cell (see Fig. 9). As shown in Table II, for $x=0.25$, the Rh-B bond length is 2.085 Å while for $x=0.5$ in the lowest-energy configuration, the Rh-B bond length becomes 2.076 Å. The shortening of these strong covalent bonds leads to strengthening of the bonds and an increase in the bulk modulus. The displacement of Rh ions as well as an increase in the lattice constant reduces hybridization of Rh 4*d* orbitals with those of Sc and consequently the covalent bonding contribution, and leads to an increase in the ionic character.

Interestingly in the lowest-energy configuration for $x=0.5$ the Rh ions are displaced by 0.069 Å away from B atoms in a symmetrical fashion as there are no B atoms in the adjacent cubes and the strain in the atomic structure is minimal. In other configurations some B atoms occupy centers of nearest-neighbor cubes, which is not optimal, and it has the effect of reducing the bulk modulus. When x is further increased to 0.75, the Rh-B bond lengths become 2.035, 2.037, 2.038, 2.040, 2.102, and 2.106 Å and also there is a significant increase in the lattice constant (Table II). This results in partial weakening of Rh-B covalent bonds and a decrease in the bulk modulus. Also the inner Sc ions are displaced by 0.046 Å. However, for $x=1$, the Rh-B bond length decreases to 2.063 Å but the lattice constant increases to 4.125 Å compared to 4.014 Å for $x=0.5$. This leads to an increase in the covalent bonding between Rh and B but a decrease in the ionic-covalent bonding contribution between

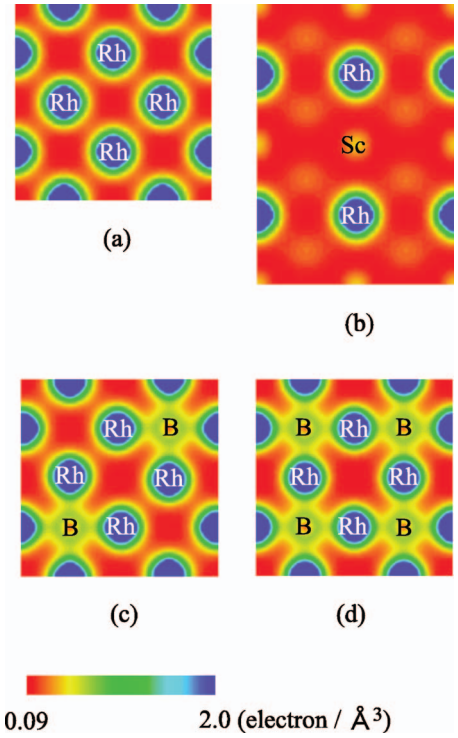

FIG. 8. (Color) Electronic charge density plots in (001) plane passing through the cube center of a cell for (a) $ScRh_3$, (c) $ScRh_3B_{0.5}$ (lowest-energy configuration), and (d) $ScRh_3B$. (b) shows the density in (011) plane in which Sc atoms can also be seen. The low electronic charge density around Sc is clear. The highest charge density appears close to the core of the Rh ions and has the value of about 4.6 electron/Å^3. However, in the figure we have used the values up to 2.0 electron/Å^3 to clarify the covalent bonding between Rh and B.

Sc and Rh. The bulk modulus increases but it is slightly lower than the value in the case of $x=0.5$. Therefore, the changes in the bulk modulus with boron doping are related to variation in the strong Rh-B covalent bonds as well as the ionic-covalent interactions between Rh and Sc. An increase in the lattice constant decreases the ionic as well as covalent contribution to cohesion between Sc and Rh while a decrease in Rh-B bond length increases the bonding contribution.

We would like to make a note of caution here that vacancies can also enhance the mechanical strength of a solid by pinning dislocations. Therefore the hardening of a solid by

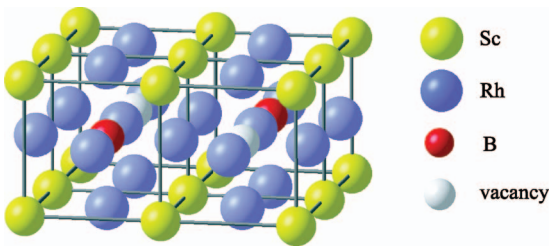

FIG. 9. (Color) The optimized positions of atoms in the $2\times2\times2$ supercell (only half the supercell is shown for clarity) corresponding to the lowest-energy configuration shown in Fig. 2(g) for $x=0.5$. Displacement of Rh ions by B toward the vacancy site can be seen.

TABLE II. Lattice constant, Rh-B and Rh-vacancy (v) bond lengths, and the corresponding number of bonds (n) for $ScRh_3B_x$. Displacement of Sc from the ideal position and the corresponding number of atoms (n) are also shown. The indexing of the configuration in the column of x is defined in Fig. 2.

x	Lattice constant (Å)	Rh-B (n) (Å)	Rh-v (n) (Å)	Displacement of Sc from the ideal position (Å)
0.000 (a)	3.930		1.965 (48)	0.000 (8)
0.250 (e)	3.970	2.085 (12)	1.985 (36)	0.000 (8)
0.500 (g)	4.014	2.076 (24)	2.007 (24)	0.000 (8)
0.750 (l)	4.075	2.035 (4)	1.969 (8)	0.046 (8)
		2.037 (8)	1.973 (4)	
		2.038 (8)		
		2.040 (4)		
		2.102 (4)		
		2.106 (8)		
1.000 (o)	4.125	2.063 (48)		0.000 (8)

vacancies could be much more drastic than the trend in the bulk modulus we obtained and also inferred from the measured hardness. However, there is no direct experimental data available on the bulk modulus and it is desirable to reveal the elastic properties of the present systems. Furthermore, depending upon the growth conditions, vacancies may be distributed rather randomly. Accordingly the observed bulk modulus or hardness may reveal an averaged behavior. The displacement of the Rh ions and in some cases the Sc ions suggests that consideration of larger unit cells may improve the values of the bulk modulus. Our results indicate that in the range of $x=0.25-0.75$, the bulk modulus may be nearly flat and this could be a reason that in experiments the microhardness is found to show a local maximum for $x=0.25$.

IV. SUMMARY

In summary we have performed first-principles calculations on $ScRh_3B_x$ in the perovskite structure to obtain the equilibrium lattice constants and the bulk modulus. The calculated equilibrium lattice constants are found to be in excellent agreement with the experimental results. Boron doping results in an almost continuous increase in the cohesive energy of these materials except around $x=0.75$ but the highest bulk modulus is realized not at $x=1$ but at $x=0.5$ with the configuration where boron occupies body-centered sites of perovskite cells in a tetrahedral arrangement. The origin of these properties is explained in terms of the changes in the covalent and ionic bonding characters. The density of states at the Fermi energy also shows a minimum for $x=0.5$. As boron doping displaces Rh atoms, it could be possible to achieve more optimal behavior of hardness of borides with suitable combination of R and M atoms.

ACKNOWLEDGMENTS

The authors are grateful to the staff of the Center for Computational Materials Science of IMR, Tohoku University, and the Center for Computational Science and Systems of the Japan Atomic Energy Agency (JAEA) for their continuous support of the computing system. This research has been partially carried out by using ITBL (IT Based Laboratory) environment. V.K. thankfully acknowledges the hospitality at IMR and RICS as well as the support from NAREGI Nano Science Project funded by the Ministry of Education, Culture, Sports, Science and Technology, Japan at RICS, AIST.

*Electronic address: sahara@imr.edu

[1] F. Galasso, *Perovskites and High-T_c Superconductors* (Gordon and Breach, London, 1990).

[2] *Solid State Ionics*, edited by H. Iwahara, M. Balkanski, T. Takahashi, and H. L. Tuller (Elsevier, Amsterdam, 1992).

[3] N. Kamegashira, J. Meng, T. Murase, K. Fujita, H. Satoh, T. Shishido, and T. Fukuda, in *10th International Ceramics Congress—Part A*, edited by P. Vincenzini (Techna Srl, Italy, 2003), p. 181.

[4] K. Oikawa, T. Kamiyama, S. Ikeda, T. Shishido, and S. Yamaguchi, Solid State Ionics **154-155**, 641 (2002).

[5] P. Rogl and L. Delong, J. Less-Common Met. **91**, 97 (1983).

[6] T. Shishido, J. Ye, T. Sasaki, R. Note, K. Obara, T. Takahashi, T. Matsumoto, and T. Fukuda, J. Solid State Chem. **133**, 82 (1997).

[7] T. Shishido, J. Ye, S. Okada, K. Kudou, T. Sasaki, S. Ishida, T. Naka, M. Oku, I. Higashi, H. Kishi, H. Horiuchi, and T. Fukuda, J. Alloys Compd. **280**, 65 (1998).

[8] T. Shishido, J. Ye, S. Okada, K. Kudou, T. Sasaki, S. Isida, T. Naka, M. Oku, I. Higashi, H. Kishi, H. Horiuchi, and T. Fukuda, J. Alloys Compd. **309**, 107 (2000).

[9] T. Shishido, K. Kudou, S. Okada, J. Ye, A. Yoshikawa, T. Sasaki, M. Oku, H. Horiuchi, I. Higashi, S. Kohiki, Y. Kawazoe, and K. Nakajima, Jpn. J. Appl. Phys., Part 1 **40**, 6037 (2001).

[10] T. Shishido, J. Ye, S. Okada, K. Kudou, M. Oku, K. Obara, T. Sugawara, A. Yoshikawa, Y. Ishizawa, M. Ogawa, K. Iizumi, I. Higashi, T. Amano, S. Kohiki, Y. Kawazoe, and K. Nakajima, Jpn. J. Appl. Phys., Part 1 **41**, 3031 (2002).

[11] T. Shishido, Y. Ishizawa, J. Ye, S. Okada, K. Kudou, K. Iizumi, M. Oku, M. Tanaka, A. Yoshikawa, A. Nomura, T. Sugawara, S. Tozawa, K. Obara, S. Oishi, N. Kamegashira, T. Amano, R. Sahara, V. Kumar, H. Horiuchi, S. Kohiki, Y. Kawazoe, and K. Nakajima, J. Alloys Compd. **408-412**, 375 (2006).

[12] T. Shishido, J. Ye, S. Okada, K. Kudou, K. Iizumi, M. Oku, Y. Ishizawa, R. Sahara, V. Kumar, A. Yoshikawa, M. Tanaka, H. Horiuchi, A. Nomura, T. Sugawara, K. Obara, T. Amano, S. Kohiki, Y. Kawazoe, and K. Nakajima, J. Alloys Compd. **408-412**, 379 (2006).

[13] R. E. Schaak, M. Avdeev, W. L. Lee, G. Lawes, H. W. Zandbergen, J. D. Jorgensen, N. P. Ong, A. P. Ramirez, and R. J. Cava, J. Solid State Chem. **177**, 1244 (2004).

[14] M. L. Cohen, Phys. Rev. B **32**, 7988 (1985).

[15] D. M. Teter, MRS Bull. **23**, 22 (1998).
[16] S. H. Jhi and J. Ihm, Phys. Rev. B **56**, 13826 (1997).
[17] S. H. Jhi, J. Ihm, S. G. Louie, and M. H. Cohen, Nature (London) **399**, 132 (1999).
[18] S. H. Jhi, S. G. Louie, M. L. Cohen, and J. Ihm, Phys. Rev. Lett. **86**, 3348 (2001).
[19] P. Ravindran, S. Sankaralingam, and R. Asokamani, Phys. Rev. B **52**, 12921 (1995).
[20] M. Oku, T. Shishido, T. Shinohara, T. Fukuda, Q. Sun, Y. Kawazoe, and K. Wagatsuma, J. Alloys Compd. **339**, 317 (2002).
[21] D. Music, Z. Sun, and J. M. Schneider, Phys. Rev. B **71**, 052104 (2005).
[22] R. Sahara, T. Shishido, V. Kumar, and Y. Kawazoe, Comput. Mater. Sci. **36**, 12 (2006).
[23] G. Kresse and D. Joubert, Phys. Rev. B **59**, 1758 (1999).
[24] P. E. Blöchl, Phys. Rev. B **50**, 17953 (1994).
[25] G. Kresse and J. Hafner, Phys. Rev. B **47**, R558 (1993); **49**, 14251 (1994).
[26] G. Kresse and J. Fürthmuller, Phys. Rev. B **54**, 11169 (1996).
[27] G. Kresse and J. Hafner, J. Phys.: Condens. Matter **6**, 8345 (1994).
[28] M. C. Payne, M. P. Teter, D. C. Allan, T. A. Arias, and J. D. Joannopoulos, Rev. Mod. Phys. **64**, 1045 (1992).
[29] J. P. Perdew, in *Electronic Structure of Solids '91*, edited by P. Ziesche and H. Eschrig (Akademie-Verlag, Berlin, 1991).
[30] F. D. Murnaghan, Proc. Natl. Acad. Sci. U.S.A. **30**, 244 (1944).
[31] Following the present study, we studied the effect of carbon doping in the case of the cubic $ScRh_3B_xC_{1-x}$ system. Replacing boron by carbon, which corresponds to increasing electron density, does not change the general features of the total DOS of the present system. In this case, E_F shifts to the right side monotonically with decreasing x, and it lies in the pseudogap in the case of $x=1$. These results will be published elsewhere.